Nucleic Acids Symposium Series No. 49 203–204

Luminescence anisotropy-based detection of nucleic acids and proteins using long-lifetime Ru(II) complex as a luminescent label

Takashi Sakamoto[1], Atsushi Mahara[2], Kobori Akio[1], Tetsuji Yamaoka[2] and Akira Murakami[1]

[1]Department of Polymer Science and Engineering, Kyoto Institute of Technology, Sakyo-ku, Kyoto 606-8585, Japan and [2]Department of Biomedical Engineering, Advanced Medical Engineering Center, Cardiovascular Center Research Institute, 5-7-1 Fujishirodai, Suita, Osaka 565-8565, Japan

ABSTRACT

Luminescence anisotropy-based methods are powerful tool for the detection of biomolecules in homogeneous physiological media without Bound/Free separation. However, analyses based on the method are always disturbed by the autofluorescence from biological specimen. This disturbance limits the sensitivity of the method. To improve the detection limit of the method, a long-lifetime luminophore was adopted as the label. Because of the lifetime of the autofluorescence is below 10ns, it is expected that the use of the long-lifetime luminophore enables us to avoid the disturbance by adopting time-resolved luminescence anisotropy measurement. To verify this concept, oligodeoxyribonucleotides and *Staphylococcus aureus* protein A were labeled with Ru(II) complex (τ~500nsec) and used for the detection of *Escherichia coli* 16S ribosomal RNA (16S rRNA) and immunoglobulin G (IgG), respectively. Results indicated that the methods were useful for the detection of rRNA and IgG without disturbance of the autofluorescence.

INTRODUCTION

Recent advancements of the methods for the detection of biomolecules largely contribute to understand the functions of DNAs, RNAs and proteins. Especially, solid-phase methods such as DNA chip[1] and oligonucletide microarray[2] enabled us to understand gene functions. These methods will play an important part of genome-based diagnostics. However, as the chip-based technology requires a lot of time-consuming procedures, the technology is not applicable for the real-time analysis of the biomolecules. For the real-time detection of biomolecule, further developments of the solution-phase methods are still required for the detection of biomolecules.

In this study, as a method to detect biomolecules in homogeneous physiological media, we adopted the luminescence anisotropy-based method. During the past 50 years, this method has contributed significantly to biological studies. This method can analyse not only the rotational motion of the luminescent-labeled biomolecule but also the change in rotational motion caused by interactions between biomolecules in homogeneous physiological media without Bound/Free separation. However, the analysis based on this method was frequently disturbed by the autofluorescence from biological specimen.

To apply this method for highly sensitive and real-time detection of biomolecules, we adopted the time-resolved luminescence anisotropy (TR-LA) analysis using long-lifetime Ru(II) complex as a luminescent label. The disturbance caused by the autofluorescence could be avoided by the TR-LA analysis using the appropriate time window. In this report, interactions between oligonucleotide (ODN) and *Escherichia coli* 16S ribosomal RNA (16S rRNA), and between *Staphylococcus aureus* protein A (SpA) and immunoglobulin G (IgG) were examined by this method.

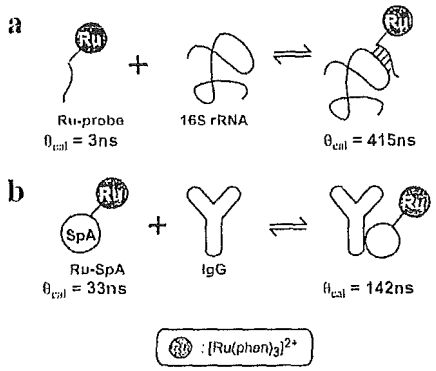

Fig. 1. Schematic illustrations of the change in rotational correlation time (θ) of Ru-probe (a) and Ru-SpA (b).
θ_{cal} was calculated according to the following equation[3];
$\theta_{cal} = (\bar{v}+h)\eta Mw/RT$
$\bar{v}$: specific volume, h: hydration volume, η: viscosity, Mw: molecular weight, R: ideal gas constant, T: absolute temperature.

RESULTS AND DISCUSSION

Ru(II) complex labeling of ODN and SpA

Ru(II) complex was successfully conjugated to the 5' end of ODN (5'-GCCGTACTCC-3'; 10mer) according to the following procedure. The sequence of the ODN was complementary to the single stranded region of 16S rRNA. The 5' end of the ODN on the CPG support was activated

by 1,1-carbonyldiimidazole and the CPG was suspended in 0.1M $[Ru(phen)_2(phen\text{-}(CH2)_5\text{-}NH_2](PF_6)_2$ in dry DMSO (60°C, 30h). After the cleavage and deprotection, the Ru(II) complex-labeled ODN (Ru-probe) was purified by reversed-phase HPLC. It was found that approximately 80% of the ODN was labeled with Ru(II) complex. SpA was labeled according to reported procedure[4]. Briefly, SpA was treated with *N*-hydroxysuccinimide activated $[Ru(phen)_2\ (phen\text{-}(CH_2)_2\text{-}CO_2H)](PF_6)_2$ in 50mM Na-carbonate buffer (pH9.8) containing 50%(v/v) DMF (20°, 18h). Unreacted Ru(II) complex and DMF were then removed by gel-filtration (Sephadex-G25). Dye to protein ration of the Ru(II) complex-labeled SpA (Ru-SpA) was 0.97. The Ru-SpA was used without further purification.

Detection of 16S rRNA and IgG by TR-LA analysis

Basic principles of the luminescence anisotropy-based detection of 16S rRNA and IgG were shown in Fig.1. In our previous study, we demonstrated that the target site of Ru-probe was accessible site for ODN binding[5]. The TR-LA analysis of Ru-probe was performed in the absence and presence of 16S rRNA (Fig.2). Results indicated that the addition of 16S rRNA to the Ru-probe caused significant change in luminescence anisotropy 0.1μsec after the pulse excitation (Fig.2, dashed line). The results suggested that the autofluorescence (τ <10nsec) from biological specimen could be avoided by the use of appropriate time window for the analysis. Rotational correlation time (θ) of Ru-probe bound to 16S rRNA was observed to be 1.2μsec, which was 3-fold greater than the calculated value (θ_{cal}) as depicted in Fig.1a, suggesting that the assumption in the calculation of θ_{cal} ($\bar{v}$+h = 1.9)[3] should be reconsidered.

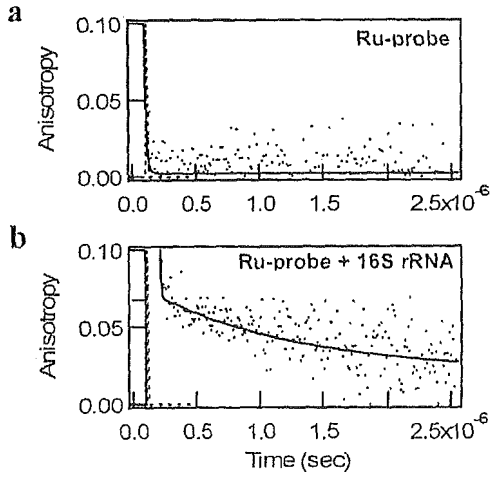

Fig.2. Luminescence anisotropy decay curves of Ru-probe in the absence (a) or presence (b) of 16S rRNA.
Dashed line represents the intensity decay of the excitation pulse. [Ru-probe]=[16S rRNA]=0.75μM in 10mM Tris-HCl (pH7.5) containing 100mM NaCl and 1mM $MgCl_2$. Measurements were carried out at 11°C

Table 1 Detection of IgG by TR-LA and SS-LA analyses using Ru-SpA in DMEM containing 10% FBS

	Luminescence anisotropy	
	TR-LA (average anisotropy) [a]	SS-LA
Ru-SpA	0.025	0.097
Ru-SpA + 0.5μM IgG	0.066	0.084
Ru-SpA + 5.0μM IgG	0.116	0.093

[a]Average anisotropy was calculated using the anisotropy decay curve 50-100nsec after the pulse excitation. [Ru-SpA]=0.3μM in 20mM PBS. Measurements were carried out at 20°C.

To evaluate the availability of the TR-LA-based detection of IgG using Ru-SpA, TR-LA analysis was compared with the steady-state luminescence anisotropy (SS-LA) analysis (Table 1). In the case of SS-LA analysis, the addition of IgG to Ru-SpA did not show the significant change in luminescence anisotropy, suggesting that the autofluorescence from FBS greatly disturbed SS-LA analysis. On the other hand, the significant change in luminescence anisotropy was detected in the case of TR-LA analysis. These results suggested that the autofluorescence from FBS was effectively avoided by the TR-LA analysis.

CONCLUSION

In this report, we tried to evaluate the availability of the TR-LA-based method for the detection of various biomolecules in the homogeneous physiological media. Results suggest that the autofluorescence due to concomitant materials in the serum containing media was effectively avoided. This methodology might contribute to the development of highly sensitive and real-time detection system for biomolecules in homogeneous physiological media.

REFERENCES

1. Schena, M., Shalon, D., Davis R.W., Brown, P.O. (1995) *Science*, 270, 467-470.
2. Yershov, G., Barsky, V., Belgovskiy, A., Kirillov, E., Kreindlin, E., Ivanov, I., Parinov, S., Guschin, D., Drobishev, A., Dubiley, S., Mirzabekov, A. (1996) *Proc. Nat. Acad. Sci. USA*, 93, 4913-4918.
3. Lakowicz, J.R. (1999) *Principles of Fluorescence Spectroscopy, 2nd Ed.* Kluwer Academic/Plunum Publishers.
4. Sakamoto, T., Mahara, A., Yamagata, K., Iwase, R., Yamaoka, T., Murakami, A. (2004) *Anal. Biochem.*, 329, 142-144.
5. Sakamoto, T., Mahara, A., Iwase, R., Yamaoka, T., Murakami, A. (2005) *Anal. Biochem.*, 340, 369-372.

Nucleic Acids Symposium Series No. 49 331–332

Synthesis and properties of photo-reactive antisense oligonucleotides containing 2'-*O*-psoralen-conjugated adenosine

Maiko Higuchi[1], Asako Yamayoshi[2], Akio Kobori[1], Tetsuji Yamaoka[3] and Akira Murakami[1]
[1]Department of Polymer Science and Engineering, Kyoto Institute of Technology, Matsugasaki, Sakyo-ku, Kyoto 602-0841, Japan, [2]Institute of Materials Chemistry and Engineering, Kyushu University, 6-10-1, Hakozaki, Higashi-ku, Fukuoka 812-8581, Japan and [3]Advanced Medical Engineering Center, National Cardiovascular Center Research Institute, 5-7-1 Fujishirodai, Suita, Osaka 565-8565, Japan

ABSTRACT

In order to selectively regulate mRNA having a point mutation, the photo-reactive antisense oligonucleotides were developed. Two types of photo-reactive oligonucleotides containing adenosine whose 2'-OH was modified with 4,5',8-trimethylpsoralen (psoralen) were synthesized (2'-Ps-oligo). One contains psoralen *via* a methylene linkage (2'-Ps-met), and the other *via* an amidomethylene linkage (2'-Ps-amd). 2'-Ps-oligos were then subjected to the photo-cross-linking reaction. 2'-Ps-met cross-linked to the complementary RNA and scarcely did to the RNA having a single mismatch base. Contrarily, 2'-Ps-amd did not cross-link to both RNA strands. These results suggest the structure of the linkage might affect the efficiency of the photo-cross-linking.

INTRODUCTION

Through the identification of human genome sequence and the development of molecular biology, it has found that various serious diseases were caused by the consequence of a single point mutation in the coding region. For example, *ras* oncogene having a single point mutation in the coding region is responsible for the transformation [1,2]. The mutation affects the cellular proliferation and induces tumorigenic properties. It is desired to inhibit selectively the expression of disease-causing mutation without affecting normal genes. Traditional drugs have certain limitations for such diseases because of the lack of the sequence specificity. The antisense strategy which inhibits gene expression in a sequence specific manner might be suitable for the purpose.

We designed new photo-reactive antisense oligonucleotides to suppress the expression of mRNA having a single point mutation and 4,5',8-trimethylpsoralen (psoralen) was adopted as the photo-reactive molecule.

In our previous study, it was found that 5'-*O*-psoralen-conjugated oligonucleotide (5'-Ps-oligo) [3] which was complementary to HPV18 mRNA inhibited the cellular proliferation of cervical carcinoma cells (C4II) upon UVA-irradiation [4]. However, there is some possibility that the psoralen of 5'-Ps-oligo could photo-cross-link to the undesired sites of mRNA because of the flexibility of the linkage. In this study, photo-reactive oligonucleotides whose 2'-OH was modified with psoralen were designed to overcome the problem.

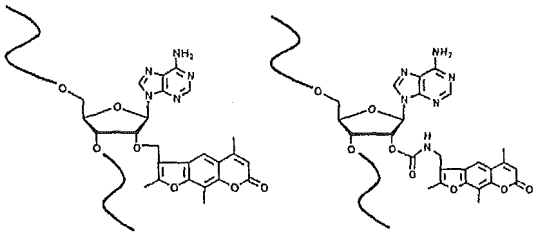

2'-Ps-met 2'-Ps-amd

Fig.1. Structures of 2'-Ps-oligos (2'-Ps-met and 2'-Ps-amd)

RESULTS AND DISCUSSION

We designed the photo-reactive antisense molecule so as to cross-link to pyrimidine base at the site of the point mutation in the target RNA, and so as not to randomly cross-link to the pyrimidine bases. The antisense molecules possess a psoralen derivative at 2'-position *via* either a methylene linkage (2'-Ps-met) or an amidomethylene linkage (2'-Ps-amd). The conformational calculation of the hybrid between 5'-Ps-oligo or 2'-Ps-oligo and its complementary RNA was carried out using AMBER* force field in MacroModel ver.8.0. It was demonstrated that both psoralens of 2'-Ps-met and 2'-Ps-amd intercalated only between the designated base pairs. Contrarily, the psoralen of 5'-Ps-oligo intercalated between the designated base pairs and also between the neighboring base pairs. This might cause the undesired cross-linking. The calculated distances between the double bond of the pyrimidine base 5-6 and the double bond of psoralen 3-4 were 5.7Å in the 2'-Ps-met and 4.0Å in the 2'-Ps-amd.

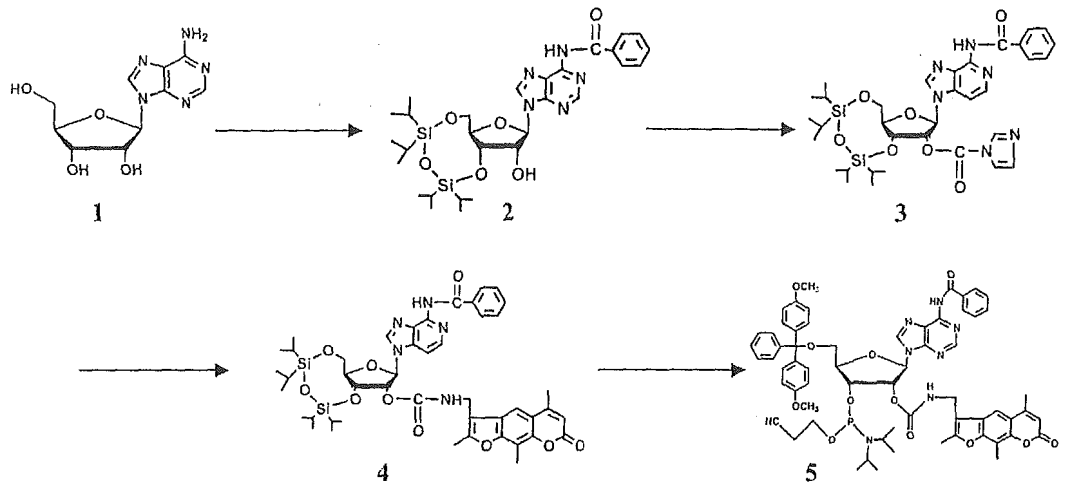

Scheme 1. Synthetic scheme of 2'-Ps-amd-adenosine derivative

Two types of 2'-*O*-psoralen-conjugated adenosine phosphoramidites were synthesized. The introduction of psoralen derivatives to the 2'position was achieved in two ways. (I) 4'-Chloromethyl-4,5',8-trimethylpsoralen was selectively introduced to 2'-position of adenosine whose 2'-OH and 3'-OH were activated by sodium hydride. (II) 4'-Aminomethyl-4,5',8-trimethylpsoralen (AMT) was introduced to 2'-position of N^6-benzoyl-3',5'-*O*-(tetraisopropyldisiloxane-1,3-diyl)adenosine **2** adopting the carbonyl diimidazole (CDI) activation protocol (Scheme1) [5]. The reaction of **2** with CDI in THF gave 2'-*O*-(imidazol-1-ylcarbonyl)-3',5'-*O*-(tetraisopropyldisiloxane-1,3-diyl)adenosine **3** in nearly quantitative yield. Subsequently, **3** was treated with AMT in THF to give **4** and **4** was isolated by column chromatography (87%). These 2'-*O*-psoralen-conjugated adenosine derivatives (Aps) were introduced to oligonucletide by the solid phase synthesis protocol. The sequence of the Ps-oligo was d(CCTCGACApsACCGCAT), which was complementary to codon12 of K-ras mRNA surrounding region.

2'-Ps-oligos were then subjected to the photo-cross-linking reaction with their target RNAs. The reactions were analyzed by RPLC and denaturing PAGE. 5'-Ps-oligo cross-linked to both its complementary RNA and RNA having a single mismatch base. It means that 5'-Ps-oligo could cross-link to the undesired site of RNA. On the other hand, 2'-Ps-met cross-linked to its complementary RNA upon UVA-irradiated, but scarcely cross-linked to the RNA having a single mismatch base. These results suggest that 2'-Ps-met could selectively cross-link to the site of a single base mutation of RNA.

CONCLUSION

We reported the synthesis of photo-reactive antisense oligonucleotides containing 2'-*O*-psoralen-conjugated adenosine. Photo-cross-linking reaction studies indicated 2'-Ps-met has higher selectivity than 5'-Ps-oligo, and 2'-Ps-met becomes a powerful antisense molecule to inhibit the expression of mRNA.

REFERENCES

1. Barbacid,M. (1987) *Ann .Rev. Biochem.*, **56**, 779-827.
2. Bos,L. (1989)*Cancer Res.*, **49**, 4682-4689.
3. Murakami, A., Yamayoshi, A., Nishida, J., Iwase, R., Yamaoka, T. and Wake, N. (2001) *Eur. J. Pharm. Sci.*, **13**, 25-34.
4. Lee.B., Murakami.A., Blake.K., Lin.S., Miller. P. (1988) *Biochemistry*, **27**, 3197-3203.
5. Korshun.V., Stetsenko.D., Gait.M. (2002) *J. Chem. Soc.,Perkin Trans. 1*, 1092-1104.

Nucleic Acids Symposium Series No. 49 151–152

Synthesis of antisense oligonucleotides containing a photocleavable protecting group on a guanine base and their photoinduced duplex formation

Reiko Iwase[2], Udai Fukui[1], Akio Kobori[1], Tetsuji Yamaoka[3] and Akira Murakami[1]

[1]Department of Polymer Science and Engineering, Kyoto Institute of Technology, Matsugasaki, Sakyoku, Kyoto, 606-8585, Japan, [2]Department of Biosciences, Teikyo University of Science and Technology, 2525 Yatsusawa, Uenohara, Yamanashi, 609-0193, Japan and [3]Department of Biomedical Engineering, Advanced Medical Engineering Center, National Cardiovascular Center Research Institute, 5-7-1 Fujishirodai, Suita, Osaka, 565-8565, Japan

ABSTRACT

An oligonucleotide containing a photocleavable protecting group at a guanine base was synthesized to induce the duplex formation by photo-irradiation. α-Methyl-2-nitropiperonyl (MeNP) group was used for the photocleavable protecting group at O^6 position of deoxyguanosine. The oligonucleotide containing MeNP group (MeNP-ODN:5'-dTTCTG^{MeNP}TCTGT-3') was synthesized by phosphoramidite method. The MeNP group was found to be removable by UV irradiation at wavelength of 365 nm for 5 min in 98% yield. UV-melting temperature (Tm value) analysis indicated that the duplex of MeNP-ODN with the complementary RNA was significantly unstable compared with the unmodified DNA/RNA duplex(⊿Tm= -25 ℃). After UV irradiation at 365 nm, the Tm value of the mixture increased to the same as that of the unmodified duplex. These results suggest that the RNA binding ability of the MeNP-ODN can be induced by photocleavage of the MeNP group.

INTRODUCTION

Phototriggered duplex formation of oligonucleotides with the target DNA and RNA is expected as a new means for the temporal and spatial control of gene expression by photo-irradiation. Recently, systems for the phototriggered duplex formation of oligonucleotides have been reported by the use of photoinduced conformational change of azobenzene group[1] or photocleavage of 1-*o*-nitrophenyl-1,3-propanediol linker[2] on the modified oligonucleotides. The control of base-pair formation of oligonucleotides using photocleavable protecting groups on the thymine bases has been reported to induce the duplex formation by photo-irradiation.[3,4] We have developed the utility of 6-nitroveratryloxycarbonyl (NVOC) group[5] as a photocleavable protecting group of the N^3 position of thymidine on antisense oligonucleotides.[3] This protecting group has proved to have a property that it could be removed by photo-irradiation at wavelength of 365 nm to induce the T-A base pairing of the oligonucleotide with the complementary RNA. Unfortunately, the photocleavage of the NVOC group required 5 h. Furthermore, two NVOC groups were needed in 18-mer-antisense DNA for the sufficient destabilizing effect of the duplex formation with complementary RNA. It is therefore required to introduce faster photocleavable protecting group at more effective position on antisense DNA as compared with the NVOC-modified oligonucleotides. We have chosen α-methyl-2-nitropiperonyl (MeNP) group as a rapidly photocleavable protecting group to protect the O^6 position of deoxyguanosine for the induction of G-C base pairing by photo-irradiation (Figure 1). Recently another group has reported that rapidly photocleavable 2-(2-nitrophenyl)propyl group was attached to the O^4-position of thymidine on oligonucleotides for the photoinduced duplex formation with complementary DNA.[4] In this report, we present the synthesis of MeNP-modified oligonucleotides (MeNP-ODN) (1) and the ability of photo-induced duplex formation of MeNP-ODN with the complementary RNA.

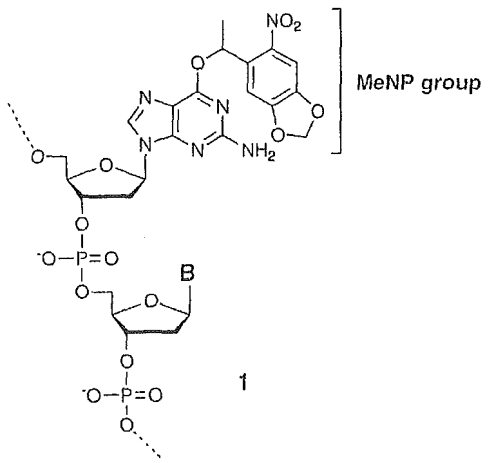

Figure 1. Structure of MeNP-modified oligonucleotide

RESULTS AND DISCUSSION

First, we prepared a deoxyguanosine phosphoramidite **5** bearing MeNP group at the O^6 position (Figure 2). 3',5'-bis-O-(t-butyldimethylsilyl)-N^2-phenoxyacethyl-2'-deoxyguanosine was first converted into 3',5'-bis-O-(t-butyldimethylsilyl)-N^2-phenoxyacethyl-O^6-mesitylene-sulfonyl-2'-deoxyguanosine in 80% yield. The intermediate was converted into the 6-quinuclidinium salt, which was allowed to react with 1-(4,5-methylenedioxy-2-nitrophenyl)ethanol in the presence of DBU to give the O^6-MeNP-modified derivative (**2**) in 86% yield. The treatment of **2** with TBAF gave the 3',5'-diol derivative (**3**) in 83% yield. The 5'-dimethoxytritylation of **3** gave the 5'-O-tritylated product **4** in 41% yield. Compound **4** was converted into **5** by 3'-phosphitylation in 81% yield.

Next, MeNP-ODN was prepared by phosphoramidite method using **5** and other nucleoside phosphoramidites bearing easily-removable protecting groups under mild basic condition at exocyclic amino functions of guanine and cytosine bases (G^{iPrPac}, C^{Ac}, T: iPrPac = *p*-(isopropyl)phenoxyacetyl, Ac = acetyl). CPG support with hydroquinone-O,O'-diacetic acid linker was also used. Cleavage from CPG and deprotection of the MeNP-ODN with 0.05M of potassium carbonate in methanol[6] for 2h gave MeNP-ODN (5'-dTTCTG^{MeNP}TCTGT-3'; G^{MeNP} = deoxyguanosine having a MeNP group at O^6 position).

The MeNP group of MeNP-ODN was found to be removable by UV irradiation at wavelength of 365 nm (transilluminator, 2.5 mW/cm^2, 37 ℃) in 5 min to produce the unmodified oligonucleotide in 98 % (Scheme 1).

To examine the destabilizing effect of the MeNP group for the duplex formation, we measured UV melting temperature (Tm value) of the mixture of MeNP-ODN and complementary RNA. The Tm value of this duplex (Tm = 16 ℃) was significantly reduced compared with that of unmodified ODN-RNA duplex (Tm = 41 ℃)(Table 1). In mixtures with complementary RNA, the MeNP-ODN also exhibited the Tm value 5 ℃ lower than the mismatch ODN (5'-dTTCTATCTGT-3') containing an adenine mismatch base (Tm = 21 ℃) (Table 1). These results suggest that the MeNP group on the oligonucleotide remarkably inhibits the duplex formation. After UV irradiation to the mixture of the MeNP-ODN with the complementary RNA, the Tm value was the same as that of unmodified duplex (Table 1). This result indicates that the RNA binding ability of MeNP-ODN was induced by UV irradiation. Thus, the photo-induced RNA binding ability of oligonucleotide was achieved by the introduction of photocleavable protecting group at the O^6 position of guanine base.

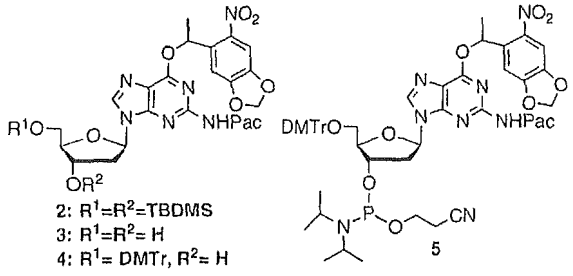

Figure 2. Structures of MeNP-modified deoxyguanosine derivatives

Scheme 1.

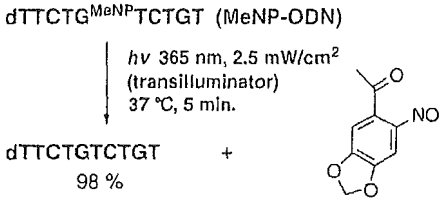

Table 1. Values of Tm for MeNP-ODN with the complementary RNA

	Tm(℃)	⊿ Tm(℃)
unmodified ODN	41	-
mismatch ODN	21	-20
MeNP-ODN	16	-25
MeNP-ODN (UV irradiation)	41	0

Measurement: 10mM phosphate buffer (pH7.0), 1M NaCl. Concentration of total oligonucleotides: 4μM. Condition of UV irradiation: transilluminator (hν/ 365nm, 2.5mW/cm^2, room temperature , 5 min.). Sequence of mismatch ODN: 5'-dTTCTATCTGT-3'.

CONCLUSION

In conclusion, MeNP group can be attached to the O^6 position of deoxyguanosine and incorporated into oligonucleotide in a site-specific manner by the use of MeNP-modified deoxyguanosine phosphoramidite unit **5**. The MeNP group on oligonucleotide has high photocleavage efficiency at UV wavelength of 365 nm and allows the production of unmodified oligonucleotide. The MeNP-modified oligonucleotide has the ability of photo-induced duplex formation with the target RNA.

REFERENCES

1. Asanuma, H., Ito, T., Yoshida, T., Liang, X., Komiyama, M.(1999) *Angew. Chem. Int. Ed.*,**38**, 2393-2395.
2. Ordoukhanian, P., Taylor, J-S. (1995) *J. Am. Chem. Soc.*, **117**, 9570-9571.
3. Iwase, R., Kitani, A., Yamaoka, T., Murakami, A. (2003) *Nucleic Acids Res. Supp.*, **3**, 61-62.
4. Kröck, L., Heckel, A. (2005) *Angew. Chem. Int. Ed.*, **44**, 471-473.
5. Alvarez, K., Vasseur, J.-J., Beltran, T., Imbach, J.-L. (1999) *J. Org. Chem.*, **64**, 6319-6328.
6. Kuijpers, W.H.A., Kuyl-Yeheskiely, E., van Boom, J.H., Boeckel, C.A.A. (1993) *Nucleic Acids Res.*, **21**, 3493-3500.

J Artif Organs (2005) 8:245–251
DOI 10.1007/s10047-005-0314-z

ORIGINAL ARTICLE

Ahamed EL-Salmawy, PhD · Tatsuya Kitagawa, MS
In Kap Ko, PhD · Akira Murakami, PhD
Yoshiharu Kimura, PhD · Tetsuji Yamaoka, PhD
Hiroo Iwata, PhD

Preparation and properties of ProNectin F-coated biodegradable hollow fibers

Abstract ProNectin F-coated biodegradable hollow fibers were newly prepared and their cytocompatibility was evaluated in vitro. Although the coating efficiency onto poly(L-lactic acid) (PLLA) and poly(lactide-co-caprolactone) [p(LA/CL)] matrices was similar, the cell adhesion properties were greatly affected by the nature of the polymer substrate. ProNectin F-coated PLLA showed about seven times higher cytocompatibility than ProNectin F-coated p(LA/CL). The single-extruded melt spinning method and the core–sheath bicomponent melt spinning method were employed to prepare PLLA hollow fibers. The effect of the spinning conditions, such as the melt draw ratio, spinneret temperature, and take-up speed, on the diameter and wall thickness of the spun fibers was studied in detail. For single-extruded melt spinning, a segmented type of spinneret was used, and the effect of the flow rate of nitrogen, which was confined in the hollow part of fibers, was studied. X-ray photographs of the drawn hollow fibers, clarified the significant molecular orientation, which was much higher than that in drawn solid PLLA fiber under identical drawing conditions. The morphology and mechanical properties of hollow fibers demonstrated an increase in the tensile strength and a decrease in the thickness of the PLLA wall with increased nitrogen flow rates and melt draw ratios for single-extruded melt spinning. These results indicate the unique characteristics of ProNectin F-coated PLLA hollow fibers, which can be successfully utilized as a biodegradable substrate.

Key words Hollow fiber · Biodegradable polyester · PLLA · Melt spinning · Smooth muscle cell

Received: April 15, 2004 / Accepted: September 9, 2005

A. EL-Salmawy[1] · I.K. Ko · H. Iwata
Institute for Frontier Medical Sciences, Kyoto University, Kyoto, Japan

T. Kitagawa · A. Murakami · Y. Kimura · T. Yamaoka[2] (✉)
Department of Polymer Science and Engineering, Kyoto Institute of Technology, Matsugasaki, Sakyo-ku, Kyoto 606-8585, Japan

Present address:
[1]Department of Apparel Design, Management and Technology, Faculty of Applied Arts, Helwan University, Giza, Egypt
[2]Department of Biomedical Engineering, Advanced Medical Engineering Center, National Cardiovascular Center Research Institute, 5-7-1 Fujishirodai, Suita, Osaka 565-8565, Japan
Tel. +81-6-6833-5012 (ext. 2637); Fax +81-6-6835-5476
e-mail:yamtet@ri.ncvc.go.jp

Introduction

Polymers used for surgical materials may be classified as biostable polymers and biodegradable polymers. In the latter group, the implanted polymer is expected to serve its supportive role, degrade to nontoxic products which are eliminated through the normal excretory routes, and finally be replaced by the surrounding tissues. Examples of such materials are poly(glycolic acid), poly(hydroxy-butyric acid), poly(L-lactic acid) (PLLA), and their copolymers.[1–4] One of the most exciting current areas for applications of biodegradable polymers is tissue engineering. Several studies have been done on these materials as a matrix for living cells. Important properties of such materials are porosity for cell in-growth, a surface that balances hydrophilicity and hydrophobicity for cellular adhesion, mechanical properties that are compatible with those of the tissue, and degradation rate.

In the past two decades, hollow fiber membranes have been utilized to culture and maintain a wide variety of transformed and primary cells. Several types of devices have been designed to sequester the cells from the surrounding tissue and yet provide bidirectional transport for cell nutrients, substrates, wastes, and key metabolites. Many research studies have dealt with the method for producing hollow fibers, and most used a dry–wet coagulation spinning process and a few used a melt-spinning process.[5,6] We have obtained various core–sheath fibers composed of different polyesters such as PLLA and poly(butylenes terephthalate) by core–sheath melt spinning processes.[7–10]

In the present study, water-soluble poly(ethylene oxide) (PEO) and PLLA were selected as core and sheath matrices, respectively, in this melt spinning process. The PEO core was removed by immersing the core–sheath fiber in water, resulting in a PLLA hollow fiber.

We also tried to establish new methods for creating biodegradable hollow fibers with high cytocompatibility; the cell adhesion properties of the biomaterial surface is important for applications in tissue engineering such as small-diameter blood vessels and guided tissue regeneration for nerve systems. Not only the mechanical properties of the hollow fibers based on their crystallinity, but also compatibility with surface-modification materials must depend on the nature of the polymeric substances used. To improve cytocompatibility, ProNectin F, which contains 13 arginine–glycine–aspartic acid (RGD) sequences interspersed between repeated glycine–alanine–glycine–alanine–serine (GAGAS) structural peptide segments derived from silk β-sheet structures, was selected as the coating material. ProNectin F is an artificially prepared protein with a molecular weight of about 110000 [sodium dodecyl sulphate-polyacrylamide gel electrophoresis (SDS-PAGE) analysis] and was produced from a synthetic gene via bacterial fermentation. This artificial polypeptide is a useful material for surface coating to form a hydrophobic surface, because its water-insoluble β-sheet structure stabilizes the coating layer. A cell adhesion test was conducted using human aorta smooth muscle cells (hAoSMCs) and bovine coronary artery smooth muscle cells (BCASMCs), which are known to interact with cell adhesion proteins such as fibronectin and RGD oligopeptides.[11] We first studied the coating compatibility and stability of ProNectin F on PLLA or poly(lactide-co-caprolactone) films, and the effect of the coating on the adhering properties of SMCs was also evaluated. According to the results, biodegradable hollow fibers with high cytocompatibility were prepared.

Materials and methods

Materials

PLLA Lacty and PEO (ALKOX R-1000, 1000Da) were supplied by Shimadzu (Kyoto, Japan) and Meisei (Kyoto, Japan), respectively. The PLLA pellets and hot pressed PEO sheets were thoroughly dried in a vacuum oven for 12h at 85° and 70°C, respectively. The melting temperature (Tm) and glass transition temperature (Tg) of PLLA were 170° and 60°C, respectively. Its number-average molecular weight (Mn) was 136000Da, having a polydispersity (Mw/Mn) of 1.74. ProNectin F was kindly donated from Sanyo Chemical Industries (Kyoto, Japan). Two types of smooth muscle cells, those derived from human aorta (hAoSMCs) and bovine coronary artery (BCASMCs), were purchased from Toyobo (Osaka, Japan) and Clonetics (San Diego, CA, USA), respectively. The hAoSMCs were cultured in Dulbecco's modified Eagle's medium (D-MEM) medium (Nissui, Tokyo, Japan) with 20% fetal bovine serum (FBS) (Sigma-Aldrich, St Louis, MI, USA), and BCASMCs were cultured in D-MEM/F12 medium (Invitrogen, Carlsbad, CA, USA) with 10% FBS (BioWhittaker, Walkersville, MD, USA).

Coating of ProNectin F onto PLLA and p(LA/CL) matrices

Cast films made of PLLA or p(LA/CL) with a diameter of 14mm and PLLA hollow fiber obtained by the single-extruded melt spinning method were used. These matrices were sterilized by immersing in 70wt% ethanol solution for 30min and dried in a safety cabinet. The sterilized samples were immersed in 20μg/ml aqueous ProNectin F solution at room temperature for 1h. After ProNectin F adsorption, the samples were thoroughly washed with phosphate-buffered saline (PBS).

Cell adhesion test

ProNectin F-coated polymer samples were placed in wells of a 24-well culture plate. SMC cells that were grown to subconfluence on polystyrene tissue culture flasks were collected by the trypsin digestion method using a 0.05% trypsin-ethylenediaminetetraacetic acid (EDTA) solution. A given volume of cell suspension (1×10^4–1×10^7 cells/ml) in serum-free culture medium was loaded into each well and incubated under 5% CO_2 at 37°C for 2h. After 2h of incubation, the cell-adhering samples were rinsed with the serum-free culture medium to remove weakly bounded cells and the cellular morphology on the films and hollow fibers was observed using a phase-contrast optical microscope (Olympus IMT-2, Tokyo, Japan). As a control experiment, the same test was done without ProNectin F coating. The number of adherent cells was counted by WST-1 assay (Dojindo, Kumamoto, Japan). The morphology of the adherent SMCs was estimated by Giemsa staining after fixation in 10% neutral buffered formaldehyde.

Melt spinning of core–sheath fibers

Five grams of PEO was placed between two aluminum plates with an aluminum spacer of 200μm in thickness and then hot pressed at 90°C at 490N for 5min. The resultant films ($10 \times 10 cm^2$) were cut into pellets and the pellets were dried in a vacuum oven for 12h at 70°C.

A spinning machine consisting of two identical 15-mm screw extruders was used to conduct the core–sheath spinning (Fig. 1a). The vertical screw extruder was used for extruding the core part, while the horizontal one was used for extruding the sheath part. The pellets of the two polymers were melted in their respective cylinders, combined in the spinneret, and then extruded through the spinneret consisting of a core nozzle of 0.5mm diameter and a sheath nozzle of 1.0mm diameter. As the extrudate left the spinneret, the fiber was melt drawn at a predetermined speed during cooling.

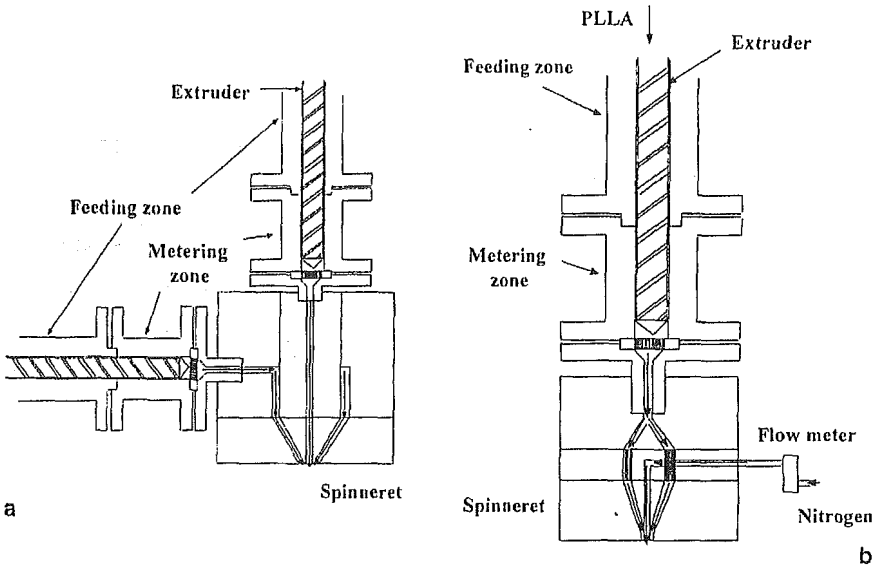

Fig. 1. Schematic illustrations of the spinnerets used for a core–sheath type hollow fibers and b single-extruded melt spinning hollow fibers. *PLLA*, poly(L-lactic acid)

Single extruding of hollow fiber

Melt spinning of a single-extruded hollow fiber was carried out in a spinning machine consisting of one 15-mm screw extruder with a specially designed nozzle for melt spinning of hollow fiber. Figure 1b shows the spinneret design; the tube-in-orifice spinneret device contained an injection tube for nitrogen with an external diameter of 1.2 mm, while the PLLA flowed through the outer orifice with a diameter of 1.7 mm. The polymer pellets were melted in the cylinder at 200°C, extruded through the spinneret, and melt drawn at a constant velocity. The as-spun fibers were then subjected continuously to the drawing stage by heating them on a hot plate kept at 80°C. The obtained drawn fibers were wound on a winder.

Measurements

Tensile properties were measured at room temperature by using a Tensilon UTM-4L tensile tester (Toyo, Tokyo, Japan). The cross-head speed was 50 mm/min and the sample length was 20 mm. Wide-angle X-ray scattering (WAXS) was carried out on a JDX 7E type X-ray diffractometer (JEOL, Tokyo, Japan). The X-rays were generated at 40 kV and 20 mA, and the Ni-filtered Cu K α radiation of 0.1542 nm wavelength was used. The fiber was wound on a sample holder so as to maintain the individual filaments parallel to each other. The exposure time was 7 h. Scanning electron microphotographs (SEM) were obtained with a JEOL JSM-25S microscope at an accelerating voltage of 5.0 kV.

Table 1. Amount of ProNectin F coating and cell adhesion onto various films

Film	ProNectin (mg/cm^2)	Adhered cells in 1 h (%)
PLLA	–	4.24 ± 3.17
Coated PLLA	0.79 ± 0.12	24.7 ± 3.58
p(LA/CL)	–	1.18 ± 0.07
Coated p(LA/CL)	0.96 ± 0.11	3.47 ± 0.53

PLLA, poly(L-lactic acid); p(LA/CL), poly(lactide-co-caprolactone)

Results and discussion

ProNectin F coating of PLLA and p(LA/CL)

To evaluate the affinity of ProNectin F and different biodegradable matrices, PLLA and p(LA/CL) were coated under the same conditions. As shown in Table 1, the amount of ProNectin F coating was almost the same for both polymers. When poly(lactide-co-glycolide) with a copolymer composition of 50/50 was coated with ProNectin F, the coating amount was much smaller than for these polymers (data not shown), indicating that matrix selection is one of the most important factors in developing new materials with high cytocompatibility. In spite of the similar coating amount for PLLA and p(LA/CL), the adhesion of hAoSMCs was greatly improved only for PLLA films (Table 1). For PLLA, cell adhesion was improved about six times, and the number of adherent cells was much larger than the coated p(LA/CL). Not only the number of adherent cells but also the shape of the adherent cells was markedly changed (Fig. 2), and hAoSMCs on the coated PLLA were more spread out. The mechanism is unclear, but there must be a big difference in the conformation of ProNectin F on these two surfaces. In general, the conformation of ProNectin F coated

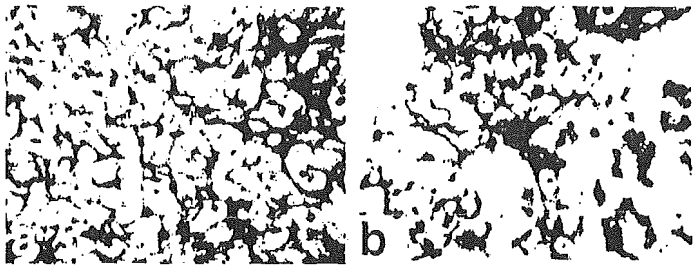

Fig. 2. Giemsa staining of the bovine coronary artery smooth muscle cells (BCASMCs) adhered on ProNectin F-coated PLLA (a) and poly(lactide-co-caprolactone) (b) films

Table 2. Tensile properties of core–sheath PLLA hollow fibers[a]

Run no.	Melt draw ratio[b] (times)	Diameter[c] (μm)		Strength (MPa)	Modulus (GPa)	Elongation (%)
		Outer	Inner			
1	10	250	190	280	3.6	60
2	12	230	180	320	4.0	40
3	15	180	150	340	4.2	40

[a]The diameters of the core and sheath nozzles were 0.5 and 1.0 mm respectively
[b]Determined by the extruding and winding speed
[c]Determined by scanning electron microscope (SEM) observation

on to a hydrophobic surface was reported to express its RGD sequence at the outer edge of the β-crystal of GAGAS sequences, but it seems to be greatly affected by the nature of the substrate, such as its hydrophobicity. According to these findings we selected PLLA as the matrix for preparing biodegradable hollow fiber.

Core–sheath type hollow fiber

Core–sheath type hollow fibers were prepared by spinning PLLA dope as the sheath and PEO dope as the core (Fig. 1a). The temperatures of the feeding zones for PLLA and PEO were set at 180° and 60°C, respectively, which are lower than the melting points of each polymer. The metering zones, in which the extruded polymers melt, were set at 190° and 80°C for PLLA and PEO, respectively. Although we have observed that the melt flow rate of PLLA achieves stability at spinneret temperatures of 210°–230°C, which are ideal conditions to attain a suitable spinnability,[8,9] the spinneret temperature was kept at 200°C for both the core and sheath because it was difficult to melt draw more than 15 times as a result of the low melt flow rate of PEO during spinning. The as-spun fibers were then drawn 5 times at 80°C, which is above the Tg of PLLA.[12–18]

Table 2 shows the tensile properties of the PLLA hollow fiber obtained by the core–sheath melt-spinning method. The outer and inner diameters of PLLA hollow fiber decreased with increasing melt draw ratio. At the maximum draw ratio of 15 times, the outer and inner diameter were 180 and 150μm, respectively. Correspondingly, the thickness of the hollow fiber wall decreased from 30 to 15μm with increasing melt draw ratio. The tensile strength and modulus of the hollow fibers slightly increased with increased melt draw ratio to a maximum of 340MPa and 4.2GPa, respectively, when the hollow fibers were melt drawn 15 times. On the other hand, the tensile elongation decreased from 60% to 40% when increasing the melt draw ratio from 10 to 15 times.

Single extruding of hollow fibers

In the single-extruding system, PLLA was extruded through the outer orifice with nitrogen flowing in the hollow inner region to obtain a homogeneous hollow fiber.[19] Thus the spinning temperature was different to that of the core–sheath type. The temperatures of the feeding zone, metering zone, and spinneret were 180°, 200°, and 230°C, respectively. At the optimum spinning conditions, it was necessary to increase the temperature of the spinneret to 230°C to allow balloon formation caused by nitrogen in the hollow part. If the temperature of the spinneret was below this, splitting of the hollow fiber occurred. The extruding speed and the melt draw ratio were 5m/min and 10 times, respectively.

Table 3 shows how the tensile properties of the single-extruded type of PLLA hollow fibers changed by changing the melt spinning conditions. The diameter of the fibers gradually increased with increasing flow rates of nitrogen. The wall thickness of the hollow fibers decreased from 50 to 25μm with increasing flow rates of nitrogen. In contrast to the core–sheath fibers, because the melt draw ratio was

Table 3. Tensile properties of single-extruded PLLA hollow fibers[a]

Run no.	Nitrogen flow rate (ml/min)	Diameter[b] (μm)		Strength (MPa)	Modulus (GPa)	Elongation (%)
		Outer	Inner			
1	3	200	100	300	3.2	70
2	4	260	180	320	3.9	60
3	5	310	260	330	4.0	60

[a]The nitrogen was flowing with an external diameter of 1.2 mm, while the flow of PLLA was through the outer orifice with a diameter of 1.7 mm. The melt draw ratio was 10
[b]Determined by SEM observation

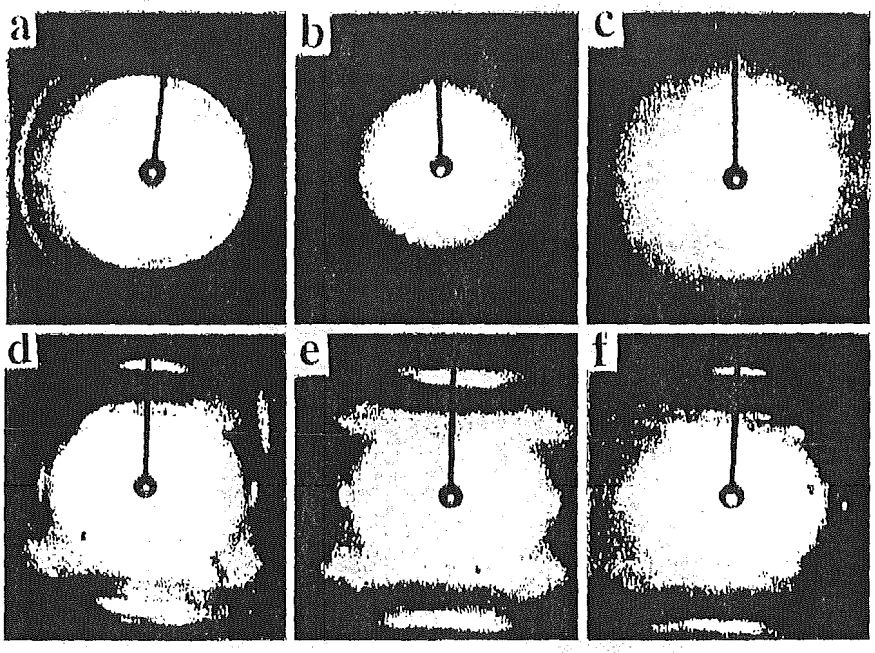

Fig. 3. Wide-angle X-ray scattering patterns of the as-spun a PLLA solid fiber, b single-extruded PLLA hollow fiber, and c core–sheath PLLA hollow fiber, and drawn d PLLA solid fiber, e single-extruded PLLA hollow fiber, and f core–sheath PLLA hollow fiber

constant (10 times), the tensile properties did not increase much. The tensile strength and modulus slightly increased on increasing the flow rate of nitrogen from 3 to 5 ml/min. In this single-extruding method, the tensile properties were a little lower than for the core–sheath melt spinning method because of the difference in the melt draw ratios (Table 2).

Crystallinity and molecular orientation of the conjugate fibers

It is well known that PLLA is a semicrystalline polymer with helical chains in its crystal structure. Figures 3a–c show the X-ray diffraction patterns of the as-spun single solid fiber, single-extruded hollow fiber, and core–sheath type hollow fiber of PLLA, respectively. Both PLLA hollow fibers in the as-spun state showed only a halo, indicating that they were amorphous and had no crystal orientation.[20–22] On the other hand, the as-spun PLLA single fiber showed many reflections as a result of its crystallinity.

Moreover, it can be observed that, under identical drawing conditions for the PLLA single solid fiber and the two types of PLLA hollow fibers, the crystal orientation increased in the hollow fibers compared to that of the single solid fiber (Figs. 3d–f). However, the crystal orientation of the core–sheath type increased sharply by the melt and hot drawing process, whereas that of the single-extruded type was not able to reach such a level of orientation. A possible explanation of the different crystal orientation behavior of the two types of drawn PLLA hollow fibers could be related to their different initial morphology; the core–sheath fibers could be melt drawn 15 times, and their tensile properties were improved by the high crystal orientation. The above results suggest that the polymer chains of the drawn PLLA hollow fibers achieve higher crystal orientation than those of the PLLA single solid fiber.

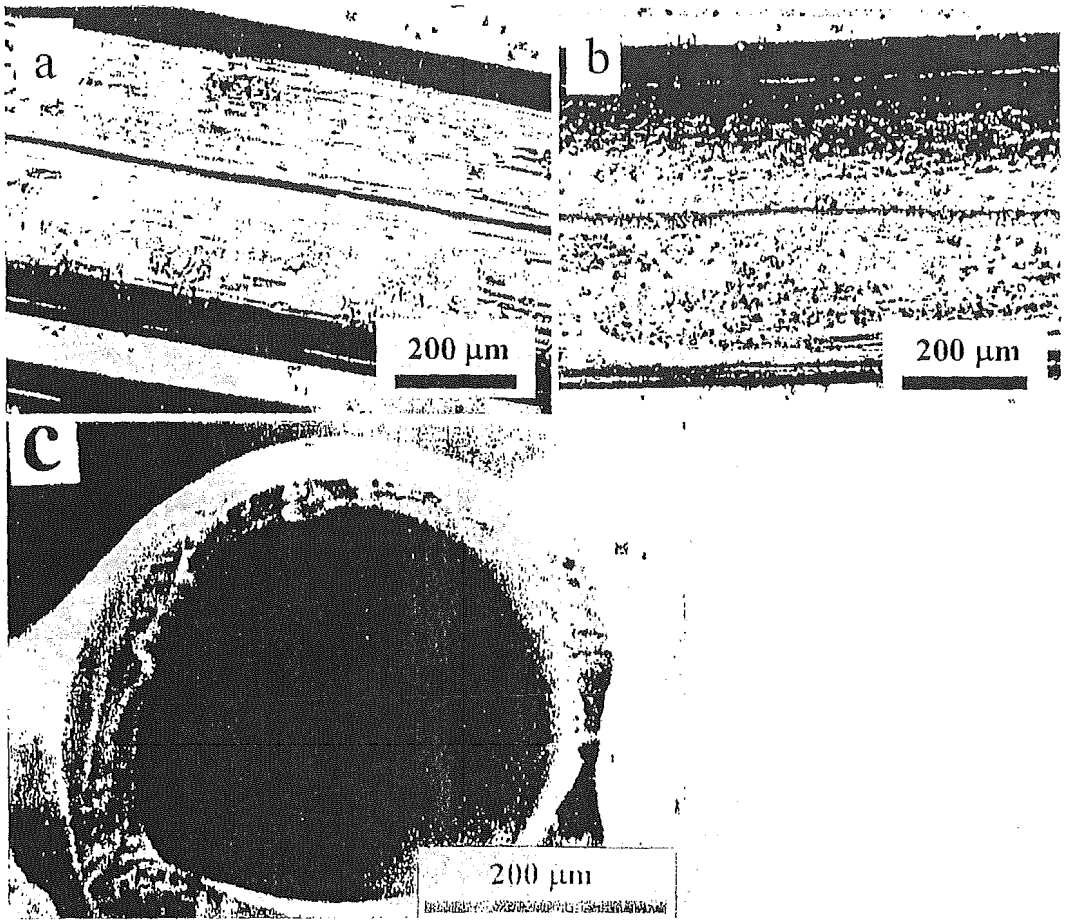

Fig. 4. Optical microphotographs of BCASMCs adhered onto a uncoated and b ProNectin F-coated PLLA hollow fibers after 2 h of incubation and c scanning electron microscope microphotographs of the as-spun PLLA hollow fiber used for the cell adhesion experiment

ProNectin F coating and BCASMC adhesion for single-extruded hollow fiber

Figures 4a and 4b show phase-contrast microphotographs of the adhering BCASMCs on the ProNectin F-coated and noncoated hollow fibers obtained by the single-extruding method (run no. 3 in Table 3). Figure 4c shows the SEM cross-section of an as-spun PLLA hollow fiber used for the cell adhesion experiment. Its smooth surface properties and quite homogeneous wall thickness can be observed. Since it is difficult to accurately measure the surface area of the hollow fiber, the number of adherent cells was not ascertained. However, the enhanced cell adhesion was clearly observed in the photographs as well as in the above experiment using PLLA films (Table 1): BCASMCs did not adhere well onto the uncoated PLLA fiber (Fig. 4b). With culture time, a few cells adhered on the uncoated fibers and grew on it; however, cells formed an irregular cell layer on the uncoated fibers. On the other hand, BCASMCs adhered well and rapidly proliferated on the ProNectin F-coated fibers. After 4 days of culture, BCASMC cells formed uniform cell layers on the fibers (data not shown).

Conclusions

We have developed the new single-extruded melt spinning technique to create biodegradable hollow fibers with excellent cytocompatibility. Under identical drawing conditions, the polymer chains of the drawn PLLA hollow fibers showed higher crystal orientation than those of PLLA single solid fibers. Both the single-extruded spinning method and the core-sheath bicomponent method promise to make a great contribution to the field of biomedical materials. The cell adhesion onto PLLA matrices was greatly increased by ProNectin F coating. Numerous applications, such as small-diameter blood vessels and guided

tissue regeneration for nerve systems, may be achievable using these biodegradable hollow fibers. We are currently trying to establish a method to increase the permeability of these hollow fibers to serve as biodegradable scaffolds, which is one of the targets of our research.

Acknowledgments This study was supported by the Industrial Technology Research Grant Program of 2000 from the New Energy and Industrial Technology Development Organization (NEDO) of Japan and by Ministry of Education, Science, Sports and Culture of Japan Grant-in-Aid for Scientific Research (B) 16300153, 2004.

References

1. Domb AJ, Wiseman DM, Kost J. Handbook of biodegradable polymers. Amsterdam: Harwood, 1997
2. Fambri L, Pegoretti A, Fenner R, Incardona DS, Migliaresi C. Biodegradable fibers of poly(L-lactic acid) produced by melt spinning. Polymer 1997;38:79–85
3. Malcolm D. The melting range of semicrystalline polymers and copolymers. J Polymer Sci 1956;19:347–352
4. Kobayashi J, Asahi T, Ichiki M, Oikawa A, Suzuki H, Watanabe T, Fukada E, Shikinami Y. Structural and optical properties of poly lactic acids. J Appl Phys 1995;77(7):2957–2973
5. Murthy NNS, Bray RG. Drawing and annealing of nylon-6 fiber: Studies of crystal growth, orientation of amorphous and crystalline domains and their influence on properties. Polymer 1995;36:3863–3873
6. Miyata K, Ito H, Kikutani T, Okui N. Fiber structured development in high-speed melt spinning of poly (ethylenetelephthatate-co-ethylene z.b-naphthalene dicarboxylate). J Polym Eng 1999;19: 395–418
7. EL-Salmawy A, Kimura Y: Environmentally friendly treatment for enzymatic scouring of conjugate core–sheath fibers. Fiber Preprints, Japan 2000;55:71
8. EL-Salmawy A, Kimura Y. Properties of a core–sheath conjugate fiber composed of poly(butylene terephthalate) and poly(L-lactic acid). Sen'i Gakkaishi 2000;56:241–248
9. EL-Salmawy A, Kimura Y. Structure and properties of bicomponent core–sheath fibers of poly(ethylene trephthalate) and biodegradable aliphatic polyesters. Textile Res J 2001;71:145–152
10. Merati AA, Konda F, Okamura M, Marui E. Effect of filament pre-tension on structural parameters and mechanical properties of core yarn friction spinning. Proceedings of the 4th Asian Textile Conference, Taipei, Taiwan, June 24–26, 1997
11. Kimura Y, Yamaoka T. Surface modification and properties of biodegradable polymers based on poly-L-lactides. In: Yui N, Terano M (eds) Surface Science of Crystalline. Tokyo: Kodansha Scientific, 1996;163–172
12. El-Salmawy A, Miyamoto M, Kimura Y. Preparing of a core–sheath bicomponent fiber of poly(butylene terephthalate)/poly(butylene succinate-co-L-lactate). Textile Res J 2000;70:1011–1018
13. Seymour R, Carraher C. Structure–property relationships in polymers. New York: Plenum, 1984
14. Horacek I, Kalisek V. polylactide I. Continuous dry spinning-hot drawing preparation of fibers. J Appl Polymer Sci 1994;54:1751–1757
15. Horacek I, Kalisek V. Polylactide. II. Discontinuous dry spinning-hot drawing preparation of fibers. J Appl Polymer Sci 1994;54: 1759–1765
16. Jeong H, Itoh H, Kikutan T. Fiber structure formation in high-speed melt spinning of nylon 6/PET bicomponent fibers. Seni Gakkai Preprints 1998(F):F–18
17. Inoue K, Sumita M, Asai M, O-oya S. Fractals and the structure of poly(L-lactic acid) in fragmentation. Seni Gakkaishi 1997;53(7): 265–271
18. Jeon H, Ito H, Kikutani T, Okui N. Effect of extraordinarily large-diameter nozzle in high-speed melt spinning of poly(ethylene trephthalate). Seni Gakkaishi 1997;53(12):540–548
19. Radharishhnan J, Takeshi K, Norimasa O. High-speed melt spinning of sheath–core bicomponent polyester: High and low molecular weight poly(ethylene terephthalate) systems. Textile Res J 1997;67(9):684–694
20. Murphy WL, Kohn DH, Moony DJ. Growth of continuous bonelike mineral within porous poly(lactide-co-glycolide) scaffolds in vitro. J Biomed Mater Res 2000;50:50–58
21. Incardona SD, Fambri L, Migliaresi C. Poly-L-lactic acid braided fibers produced by melt spinning: characterization and in vitro degradation. J Mater Sci Mater Med 1996;7:387–391
22. Hay PD, Smith MD, Cousins RB, Gaylor JDS. Oxygen transfer in a diffusion-limited hollow fiber bioartificial liver. Artif Organs 2000;4:278–288

4122 Biophysical Journal Volume 89 December 2005 4122–4128

Evaluation of Dynamic Features of *Escherichia coli* 16S Ribosomal RNA in Homogeneous Physiological Solution

Takashi Sakamoto,* Atsushi Mahara,† Koichi Yamagata,‡ Reiko Iwase,§ Tetsuji Yamaoka,† and Akira Murakami*

*Department of Polymer Science and Engineering, Kyoto Institute of Technology, Sakyo-ku, Kyoto, Japan; †Department of Biomedical Engineering, Advanced Medical Engineering Center, National Cardiovascular Center Research Institute, Suita, Osaka, Japan; ‡BMI Laboratory, Central Research Laboratories, Sysmex Corporation, Kobe, Hyogo, Japan; and §Department of Bioscience, Teikyo University of Science and Technology, Uenohara, Yamanashi, Japan

ABSTRACT There is no methodology for the estimation of the dynamic features of large-molecular-weight RNAs in homogeneous physiological media. In this report, a luminescence anisotropy-based method using a long-lifetime luminescent oligonucleotide probe for the estimation of the dynamic features of large-molecular-weight RNA is described. As a luminescent probe, Ru(II) complex-labeled oligonucleotides, which have a complementary sequence to the single-stranded regions of *Escherichia coli* 16S rRNA, were synthesized. After the hybridization of the probe to single-stranded regions of 16S rRNA, the segmental motions of the regions were evaluated by time-resolved luminescence anisotropy analysis. In 16S rRNA, the L2 site (323–332 nt) was found to be the most flexible among the seven sites chosen. From a comparison between the hybridization kinetics of oligonucleotides to these single-stranded regions and the rotational correlation times, it was suggested that the flexibility of the single-stranded region was closely correlated with the hybridization kinetics. Furthermore, results of the luminescence lifetime measurement and luminescence quenching experiments suggested that the highly flexible region was located on the surface of the 16S rRNA and that the less flexible region was located in the depths of 16S rRNA.

INTRODUCTION

The recent development of methodologies for the structural study of biomolecules enables researchers to predict interactions between biomolecules and to design effective inhibitors for particular biomolecules. Especially in structural studies of proteins, information on the correlation between function and structure has largely contributed to structure-based drug discoveries. Contrarily, the structural studies of RNA are limited to some extent due to its enormous diversity. Recently, bacterial 30S and 50S ribosomal subunits were crystallized and their three-dimensional structures were reported (1,2). As for the 50S ribosomal subunit, the relationship between the structure and the function has been revealed (3). However, these are rare examples and it will take more time to determine the three-dimensional structures of other RNAs. Furthermore, structural dynamics is an important issue for further understanding the functions of biomolecules. The dynamic features of biomolecules should be taken into consideration when analyzing the interaction between biomolecules. X-ray crystallography, which is mainly used for the determination of the structure of biomolecules (4,5), can only evaluate a static structure. To evaluate dynamic features of RNA, the development of sophisticated methods other than crystallography might contribute to the structure-based discovery of RNA-regulating molecules such as small-interference RNAs and antisense oligonucleotides. As methods for evaluating the dynamic features of biomolecules, NMR (6,7), electron paramagnetic resonance (EPR) (8,9), and fluorescence-based methods (10,11) have been reported. Nuclear spin relaxation measurement based on NMR spectroscopy using ^{1}H, ^{13}C, ^{15}N, and ^{31}P has been frequently used for the determination of the intramolecular flexibility of tRNA (12,13) and small proteins (14). The distinguishing feature of NMR is, in principle, that the method requires no specific labeling of biomolecules. However, the signal resolution limits the applicable molecular-weight range of the specimen (<20 kDa in molecular mass). EPR measurement (15) requires the spin-labeling of biomolecules at the designated site. Furthermore, NMR or EPR spectroscopy requires a large quantity of the specimen (several milligrams in weight); therefore, the applicability of these methods is limited to biomolecules that can be easily obtained. As another method to evaluate the dynamic features of biomolecules, fluorescence-based methods have been reported. Tuschl et al. delineated the conformational dynamics of hammerhead ribozyme by fluorescence resonance energy transfer analysis (10). This method is certainly useful for evaluating the structural dynamics of biomolecules. As for proteins, fluorescence anisotropy was measured using internal chromophores such as tryptophan, and the rotational correlation time (θ) derived from fluorescence anisotropy delineated the rotational motion around the tryptophan residue (16). This method has not been applied to evaluate the dynamic features of highly folded RNA.

In this study, we paid attention to the segmental motion of a single strand of folded RNA to estimate the dynamic structure of large-molecular-weight RNA (>100 kDa). We adopted time-resolved luminescence anisotropy analysis using a luminescent DNA probe to evaluate the segmental motions

Submitted March 7, 2005, and accepted for publication August 22, 2005.

Address reprint requests to Akira Murakami, E-mail: akiram@kit.ac.jp.

0006-3495/05/12/4122/07 $2.00

doi: 10.1529/biophysj.105.062455

of the single-stranded regions of the folded RNA. *Escherichia coli* 16S rRNA (16S rRNA; ~500 kDa) was used as the model folded RNA. In time-resolved luminescence anisotropy analysis, the rotational motion of the molecule is evaluated by θ. It is theoretically estimated that the θ value of single-stranded regions of 16S rRNA ranges from 100 ns to a few μs. Therefore, long-lifetime luminescence probes (10 ns to 1 μs) are required to evaluate large θ values (100 ns to 10 μs) (17). In this study, as a long-lifetime luminescent material, we adopted the Tris-1,10-phenanthroline Ru(II) complex with a lifetime in the range of 500 ns to 1 μs (18). The Ru(II) complex was conjugated to the oligodeoxyribonucleotides (Ru-probes), and the Ru-probes were successfully used as probes for the evaluation of the segmental motions of single-stranded regions of 16S rRNA.

EXPERIMENTAL

Chemicals

Ruthenium trichloride ($RuCl_3$) and organic solvents were purchased from Wako Chemicals (Osaka, Japan). 1,10-Phenanthroline was purchased from Aldrich Chemical (St. Louis, MO). 5-Nitro-1,10-phenanthroline was purchased from Tokyo Kasei Kogyo (Tokyo, Japan). Reagents for the oligonucleotide synthesis were purchased from Glen Research (Sterling, VA). A mixture of 16S and 23S rRNAs was purchased from Roche (Basel, Switzerland) and used without further purification.

Synthesis of Ru(II) complex-labeled oligodeoxyribonucleotide

The Ru(II) complex-labeled oligodeoxyribonucleotides were synthesized according to Scheme 1.

Fmoc-6-aminohexanoic acid

According to the general F-moc protection procedure (19), 6-aminohexanoic acid (0.79 g, 6 mmols) and triethylamine (0.84 ml, 6 mmols) were dissolved in MilliQ water (3 ml), and Fmoc-*N*-hydroxysuccineimide solution (1.96 g, 5.8 mmols/acetonitrile (6 ml)) was added to the solution. The reaction solution was adjusted to pH 8.5–9.0 and then stirred at room temperature. After 2 h, the solution was filtered, and 1.5 N HCl aqueous solution (~20 ml) was added to the filtrate. The resulting white precipitate was collected by filtration, and the precipitate was washed with MilliQ water, with a yield of 1.64 g (80%).

5-(Fmoc-6-aminohexaneamide)-1,10-phenanthroline

5-Amino-1,10-phenanthroline was synthesized according to a reported procedure (20). Fmoc-6-aminohexanoic anhydride was obtained from the condensation reaction of Fmoc-6-aminohexanoic acid (1.98 g, 5.6 mmols) with *N,N'*-dicyclohexylcarbodiimide (0.58 g, 2.8 mmols) in dry dichloromethane. Fmoc-6-aminohexanoic anhydride was mixed with 5-amino-1,10-phenanthroline (0.17 g, 0.9 mmols) in dry dichloromethane/acetonitrile (1:1 v/v) and stirred at room temperature for 160 h. The resulting yellow-white precipitate was collected by filtration, washed with dichloromethane/acetonitrile 1:1 (v/v), and dried in vacuo, for a yield of 0.36 g (68%).

Bis-(1,10-phenanthroline) 5-(6-aminohexaneamide)-1,10-phenanthroline Ru(II) dihexafluorophosphate

Dichloro-bis-1,10-phenanthroline Ru(II) dehydrate ($Ru(phen)_2Cl_2$) was synthesized according to the reported procedure (21). The heteroligand Ru(II) complex was synthesized according to the reported procedure (22) with some modifications. 5-(Fmoc-6-aminohexaneamide)-1,10-phenanthroline (0.053 g, 0.1 mmols) and $Ru(phen)_2Cl_2$ (0.057 g, 0.1 mmols) were dissolved in H_2O/EtOH (1:2 (v/v), 3 ml), and the solution was refluxed for 6 h. The reaction solution was evaporated to dryness, and the residue was dissolved in MilliQ water (16 ml). The unreacted 5-(Fmoc-6-aminohexaneamide)-1,10-phenanthroline and $Ru(phen)_2Cl_2$ were removed by

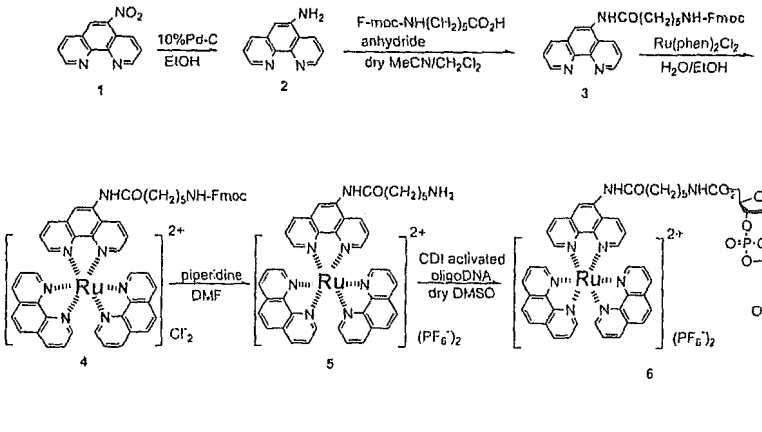

SCHEME 1

filtration, and the filtrate was evaporated to dryness. The residue was dissolved in piperidine/DMF (1:3 (v/v), 2 ml), and the solution was incubated at room temperature for 0.5 h. After evaporation, the residue was dissolved in MilliQ water (16 ml) and filtered. Then saturated NH_4PF_6 aqueous solution was added to the filtrate, and the orange precipitate that had formed was collected, yielding 0.10 g (95%).

Introduction of 5 to 5' end of oligodeoxyribonucleotides

Oligodeoxyribonucleotides (ODN, 10 mer, Table 1) were synthesized according to general cyanoethyl phosphoramidite chemistry on a controlled pore glass support. The labeling reaction was carried out on the glass support in a filter-equipped air-tight syringe. The 5' end of the ODN was activated by 1,1-carbonyldiimidazole (23), and bis-(1,10-phenanthroline) 5-(6-aminohexaneamide)-1,10-phenanthroline Ru(II) dihexafluorophosphate in dry dimethylsulfoxide (0.1 M) was added to the 1,1-carbonyldiimidazole-activated oligodeoxyribonucleotide on the glass support. After the incubation (60°C, 30 h), the glass support was washed sequentially with dimethylsulfoxide and acetonitrile. Deprotection of ODN and cleavage from the glass support were carried out according to conventional protocol. The crude solution of the Ru(II) complex-labeled ODN (Ru-probe) was purified by reverse-phase high-performance liquid chromatography with an acetonitrile gradient. Isomers of the Ru-probe were characterized by CD spectra.

Sample preparation and physical measurements

A solution of the 16S and 23S rRNA mixture (10 mM Tris-HCl (pH 7.5), 100 mM NaCl, and 1 mM $MgCl_2$) was incubated at 11°C for 24 h, and used for all sample preparations without further purification. The synthesized Ru-probe was dissolved in the same buffer solution as the rRNA and used for all sample preparations. All measurements were carried out at 11°C. The CD spectra were measured by a CD spectrophotometer (J-720, JASCO, Tokyo, Japan) equipped with a thermal controller (RET-100, Neslab, Portsmouth, NH). The melting temperatures of the hybrid of the Ru-probe and its complementary oligo-RNA were measured by a spectrophotometer (U-2000A, Hitach, Tokyo, Japan) equipped with a thermal controller. Luminescence anisotropy decay curves and emission decay curves were measured by a time-correlated single-photon counting system (NAES-550, Horiba, Kyoto, Japan) equipped with excitation (B390) and emission (Y52) filters and with a thermal controller. The luminescence spectra were measured by a spectrofluorophotometer (RF-5300PC, Shimadzu, Kyoto, Japan) equipped with a thermal controller.

TABLE 1 Sequences of Ru-probes and secondary structure of target site on 16S rRNA

	Target site	Structure around the target site	Sequence (5' to 3')
Ru-L1	L1 (887–896 nt)	internal loop	GCC GTA CTC C
Ru-L2	L2 (323–332 nt)	stem loop	CCG TGT CTC A
Ru-L3	L3 (557–566 nt)	internal loop	CAG TAA TTC C
Ru-L4	L4 (811–820 nt)	internal loop	ATC GTT TAC G
Ru-L5	L5 (1373–1382 nt)	internal loop	GAA CGT ATT C
Ru-L6	L6 (963–972 nt)	internal loop	GCG TTG CAT C
Ru-S1	S1 (634–643 nt)	stem	GTA TCA GAT G

THEORY

Time-resolved luminescence anisotropy measurement

The luminescence anisotropy decay curves ($r_{(t)}$) were calculated according to the following equation:

$$r_{(t)} = (I_{vv(t)} - G \times I_{vh(t)})/(I_{vv(t)} + 2 \times G \times I_{vh(t)}), \quad (1)$$

where the subscripts vv and vh of I indicate the orientation of the excitation and emission polarizers, respectively. For example, $I_{vv(t)}$ represents the intensity decay of the vertically polarized emission when excited by a vertically polarized light pulse. G, which is the instrumental responsive factor, was estimated from the following equation:

$$G = \sum_t I_{hv(t)} / \sum_t I_{hh(t)}. \quad (2)$$

From Eqs. 1 and 2, $r_{(t)}$ was obtained. The $r_{(t)}$ was fitted to the ideal curves represented by Eq. 3 using the nonlinear least-square deconvolution method

$$r_{(t)} = \sum_i r_{0i} \times (-t/\theta_i) + r_\infty, \quad (3)$$

where the r_{0i} are the fractional anisotropies that decay with the correlation time θ_i. The last term, r_∞, was used to account for the presence of a nonzero anisotropy at long time. From the fitted decay curve, the rotational correlation time (θ) was estimated. The predicted θ was calculated by the following equation:

$$\theta = \eta M w(h + \bar{v})/RT. \quad (4)$$

Evaluation of the Stern-Volmer constant

The emission intensity of the Ru-probe is represented by the following general Stern-Volmer equation:

$$I_{obs} = I_0/(1 + K_{sv} \times [Q]), \quad (5)$$

where I_{obs} and I_0 represent the observed emission intensity and the emission intensity in the absence of a quencher, respectively, and K_{sv} and $[Q]$ represent the Stern-Volmer constant and the concentration of the quencher in the medium, respectively. If hybridization occurs, it is assumed that two kinds of Ru-probe, i.e., free and bound probes, exist in the system. Based on this assumption, the emission intensity of the Ru-probe in the presence of 16S rRNA is represented by the following equation:

$$I_0/I = I_{0F}/I = I_{0F}/\{x \times [I_{0B}/(1 + K_{svB} \times [Q])] + (1 - x) \times [I_{0F}/(1 + K_{svF} \times [Q])]\}, \quad (6)$$

where I_{0F} and I_{0B} represent the emission intensity of the free and bound Ru-probes, respectively, K_{svF} and K_{svB} represent the Stern-Volmer constant of the free and bound Ru-probes, respectively, and x represents the binding ratio of the Ru-probe in the system. The titration curves of the quencher

molecule were fitted to Eq. 6. $K_{a,F}$ and $K_{a,B}$ were estimated from the fitted titration curves according to Eq. 6.

RESULTS AND DISCUSSION

To evaluate the rotational motion of biomolecules using time-resolved luminescence anisotropy analysis, the rotational correlation time, θ, is generally used as an indicator of the rotational motion. In our case, it was predicted that the θ value of the single-stranded regions of 16S rRNA was in the submicrosecond to microsecond range, according to Eq. 4. Therefore, to evaluate the segmental motions of the single-stranded regions of 16S rRNA, the lifetime of the luminescent probe needed to be around hundreds of nanoseconds. As a luminescent probe that could fulfill this requirement, we adopted the Ru(II) complex, the luminescence lifetime of which is ~500 ns to 1 μs. The Ru(II) complex was introduced to the 5′ end of ODN and used as a luminescent probe to evaluate the segmental motions of the single-stranded regions of 16S rRNA.

The oligonucleotide sequences of Ru-probes are summarized in Table 1. The target sites of 16S rRNA (1542 nt) were chosen on the basis of the reported secondary structure (24) (Fig. 1). The probes were purified by reverse-phase high-performance liquid chromatography, where the enantiomeric isomers (Δ and Λ isomers) were also isolated (20). The luminescence properties are summarized in Table 2. The difference in the luminescence properties between the enantiomers was negligible.

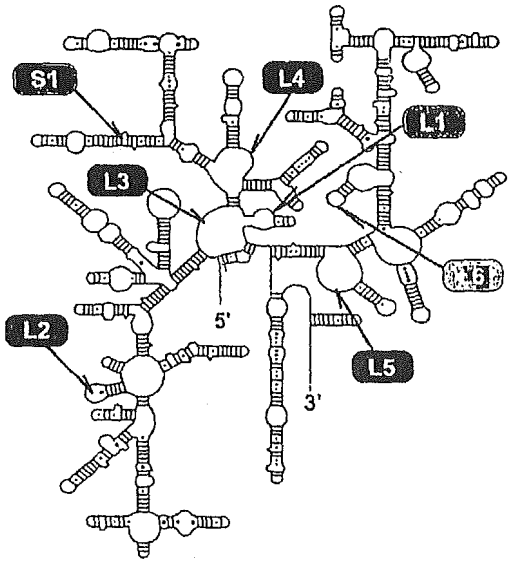

FIGURE 1 Reported secondary structure of *E. coli* 16S ribosomal RNA (24) and target sites of Ru-probes.

TABLE 2 Luminescence properties of Ru-probe

	$\lambda_{ex,max}$ (nm)	$\lambda_{em,max}$ (nm)	τ_1 (ns)	f_1	τ_2 (ns)	f_2	χ^2
Ru-probe Λ	461	587	1400	0.9	400	0.1	1.3
Ru-probe Δ	462	589	1300	0.8	100	0.2	1.4
$Ru(phen)_3^{2+}$	457	580	800	1	—	—	1.1

The oligonucleotide sequence of Ru probe is 5′ Ru-GCC GTA CTC C-3′. [Ru-probe] (or [$Ru(phen)_3^{2+}$]) = 0.75 μM in 10 mM Tris-HCl (pH 7.5) containing 100 mM NaCl and 1 mM $MgCl_2$. Measurements were carried out at 11°C.

It has been reported that Tris-1,10-phenanthroline Ru(II) complex ($Ru(phen)_3^{2+}$) interacts with double-helical DNA and that the luminescence intensity is enhanced by the interaction. It was also reported that the manner of the interaction differed for the different enantiomeric isomers of $Ru(phen)_3^{2+}$ (25). On the other hand, the binding affinity of the $Ru(phen)_3^{2+}$ to double-helical RNA was lower than that to double-helical DNA, and the enantioselectivity of the former interaction was negligible (25). Therefore, in this study, the Λ isomer was used as the luminescent probe. The emission spectrum of the Λ isomer of the Ru-probe was similar to that of $Ru(phen)_3^{2+}$, though the luminescence decay measurements showed the presence of two different lifetimes. The major component of the luminescence lifetime, τ_1, of the Ru-probe was longer than that of $Ru(phen)_3^{2+}$, suggesting that the oligonucleotide strand of the Ru-probe might interact with the $Ru(phen)_3^{2+}$ residue at the 5′ end of the oligonucleotide. As shown in Table 2, the τ_1 of the Ru-probe was long enough to evaluate the θ value of the single-stranded regions of 16S rRNA. The introduction of $Ru(phen)_3^{2+}$ to the oligodeoxyribonucleotide slightly changed the duplex stability (ΔT_m = −4–~2°C for the melting temperature estimated from the thermal denaturation curves).

To estimate the segmental motions of the single-stranded regions of 16S rRNA, the rotational correlation time (θ) of the Ru-probe/16S rRNA hybrid was measured. The anisotropy decay curves were well analyzed by a two-component exponential fitting, suggesting that there were two major luminescent species. The θ values calculated according to Eq. 3 are summarized in Table 3. The rotational correlation time, θ_2, was detected in several Ru-probes (Ru-L1, -L2, -L4,

TABLE 3 Time-resolved luminescence anisotropy analysis of Ru-probes in the presence of 16S rRNA

	θ_1 (ns)	r_{01}	θ_2 (ns)	r_{02}	r_∞	χ^2
Ru-L1 alone	9	0.06	n.d.	n.d.	n.d.	0.76
Ru-L1	6	0.09	1200	0.05	0.02	1.05
Ru-L2	18	0.03	150	0.04	0.01	1.27
Ru-L3	9	0.12	n.d.	n.d.	0.02	1.75
Ru-L4	8	0.07	590	0.05	n.d.	1.39
Ru-L5	29	0.08	380	0.01	0.05	1.10
Ru-L6	56	0.02	540	0.01	0.01	1.42
Ru-S1	22	0.11	n.d.	n.d.	n.d.	0.88

[Ru-probe] = [16S rRNA] = 0.75 μM in 10 mM Tris-HCl (pH 7.5) containing 100 mM NaCl and 1 mM $MgCl_2$. n.d., not detected.

-L5, and -L6) in the presence of 16S rRNA, whereas θ_2 was not detected in the case of the other Ru-probes (Ru-L3 and Ru-S1). This is probably due to the fact that the rotational motion of the Ru-probe was restricted and that the Ru-probe could hybridize with the single-stranded region of 16S rRNA. As the magnitude of θ_2 was different among the Ru-probes in the presence of 16S rRNA, it was suggested that each θ_2 represented the segmental motion of the single-stranded region of 16S rRNA on which the Ru-probes were hybridized. The order of magnitude of θ_2 suggested that the magnitude of the segmental motions of these sites were in the order L2 > L4 and L5 > L6 > L1. This order might provide information concerning flexibilities of the single-stranded regions of 16S rRNA in homogeneous physiological medium. That is, site L2 was the most flexible among the five sites. In almost all cases of the Ru-probes, a nonzero anisotropy at long time, r_∞, was observed in the presence of 16S rRNA. This observation is the result of the presence of slow motion(s) that display long θ(s) which cannot be observed with 0.5-~1 μs luminescence decay time Ru-probe.

To further characterize the single-stranded regions of 16S rRNA in which the Ru-probes were hybridized, the luminescence lifetimes of the Ru-probes were measured (Table 4). Three cases in which the luminescence lifetime of $Ru(phen)_3^{2+}$ increased have been reported. They are the cases when 1), the Ru complex is intercalated with the double-helical DNA (26). 2), the Ru(II) complex is isolated from quencher molecules such as solvents or salts, and 3), the Ru(II) complex is located in a high-ionic-strength environment. In all cases, it was assumed that the luminescence lifetimes of the Ru-probes that were bound to their target sites were largely concerned with the entangling of the RNA strand around the single-stranded regions of 16S rRNA where the Ru-probes hybridized. In our case, the addition of 16S rRNA caused a remarkable increase of the luminescence lifetime of Ru-L1 compared with the other Ru-probes. This result indicated at least that the entangling of the RNA strand around the L1 site was relatively high. That is, the local nucleotide density around L1 might be relatively high compared with the other sites chosen, which made sense based on the flexibility of L1.

To verify this assumption, a luminescence quenching study was performed. As a quencher molecule, potassium ferrocyanide ($K_4[Fe(CN)_6]$), which is a good quencher of Ru(II) complex derivatives (25), was adopted. Potassium ferrocyanide was added to the mixture of the Ru-probe and 16S rRNA, and the luminescence intensity was measured in the presence of various concentrations of ferrocyanide anion (Fig. 2). The resulting Stern-Volmer constants (K_{sv}) of the derivatives of the Ru(II) complex are summarized in Table 5. The K_{sv}s of the Ru-probes were lower than that of $Ru(phen)_3^{2+}$. This result suggested that the oligonucleotide strand of the Ru-probe might inhibit the access of the ferrocyanide anion to the Ru(II) complex. $K_{sv\ B}$ was detected by the addition of 16S rRNA, indicating that the binding of the Ru-probes to 16S rRNA inhibited the access of the ferrocyanide anion to the Ru(II) complexes conjugated with the oligonucleotides. The difference in $K_{sv\ B}$ of Ru-L1 and -L2 in the presence of 16S rRNA indicated that the environments around the bound Ru-probes were different between these two Ru-probes. That is, the collision frequencies of ferrocyanide anion to the Ru(II) complexes were quite different. It was assumed that the Ru(II)

TABLE 4 Luminescence lifetimes of Ru-probes in the presence or absence of 16S rRNA

	τ_1 (ns)	f_1	τ_2 (ns)	f_2	χ^2
Ru-L1	1350 (10)*	0.91	400 (70)*	0.09	1.30
+ rRNA	1690 (20)	0.80	550 (50)	0.20	1.03
Ru-L2	1300 (<10)	0.86	210 (30)	0.14	1.22
+ rRNA	1380 (10)	0.85	360 (40)	0.15	1.32
Ru-L3	1170 (<10)	0.85	60 (10)	0.15	1.54
+ rRNA	1260 (<10)	0.86	240 (30)	0.14	1.42
Ru-L4	1120 (<10)	0.84	180 (10)	0.16	1.35
+ rRNA	1270 (10)	0.82	360 (30)	0.18	1.66
Ru-L5	1210 (<10)	0.89	100 (20)	0.11	1.63
+ rRNA	1230 (<10)	0.84	280 (20)	0.16	1.64
Ru-L6	1350 (<10)	0.86	240 (20)	0.14	1.12
+ rRNA	1330 (<10)	0.84	230 (20)	0.16	1.56
Ru-S1	1300 (<10)	0.86	210 (30)	0.14	1.22
+ rRNA	1380 (10)	0.85	360 (40)	0.15	1.32

[Ru-probe] = [16S rRNA] = 0.75 μM in 10 mM Tris-HCl (pH 7.5) containing 100 mM NaCl and 1 mM $MgCl_2$. Values in parentheses indicate asymptotic standard errors.

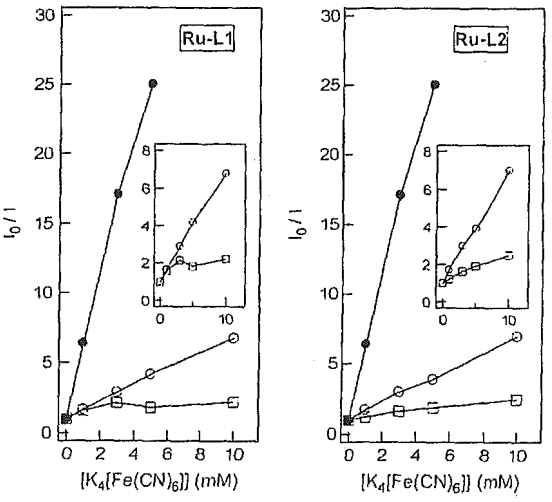

FIGURE 2 Stern-Volmer plot of the emission from Ru-probe in the presence or absence of 16S rRNA. Solid circles represent the profile of $[Ru(phen)_3]Cl_2$. Open circles and squares represent the profiles of the Ru-probe in the absence and presence, respectively, of 16S rRNA. [Ru derivative] = 0.75 μM in 10 mM Tris-HCl buffer (pH 7.5) containing 100 mM NaCl and 1 mM $MgCl_2$. The excitation wavelength was 453 nm with observation at 583 nm and a bandpass of 5 nm at 11°C.

TABLE 5 Stern-Volmer constant (K_{sv}) of Ru-probes in the presence or absence of 16S rRNA

	$K_{sv\ F}$ (M^{-1})*	$K_{sv\ B}$ (M^{-1})*	Bound ratio
Ru-L1	576	—	—
+ rRNA	576	61	0.61
Ru-L2	589	—	—
+ rRNA	589	94	0.56
$Ru(phen)_3^{2+}$	4850	—	—

*K_{sv} was estimated from Fig. 2 by the curve-fitting protocol according to Eq. 6.

complex of Ru-L2 located around its target site underwent frequent collision by ferrocyanide anion, whereas that of Ru-L1 did not. This result was in good agreement with the flexibilities of these single-stranded regions, as already discussed.

Based on the results discussed above, we proposed a novel concept for predicting the local flexibility of the single-stranded regions, which significantly affects their interaction with other biomolecules. To further verify this proposal, the flexibilities of the single-stranded regions were evaluated from the viewpoint of hybridization kinetics. We previously reported the kinetics of interactions between single-stranded regions of 16S rRNA and their complementary oligonucleotides by fluorescence anisotropy analysis using 5′-fluorescein-labeled oligonucleotides (27). In the report, we concluded that the L2 site accepted its complementary oligonucleotide far more rapidly than did the L1 site. The order of magnitude of the association rate constant (k_{assoc}) and dissociation rate constant (k_{dissoc}) of the hybridization was L2 > L6 > L1. This result suggested that a rapidly moving site, like L2, rather promptly accepts its complementary oligonucleotide, whereas a slowly moving site, like L1, reluctantly accepts its complementary oligonucleotide.

Taking these results into consideration, it seems that the L1 site was located in the depths of the 16S rRNA, and that the L2 site was on the relatively outer region of 16S rRNA. Such information is of great importance in the designing of RNA-acting molecules. Some molecules might interact with the stem regions and some with the single-stranded ones. Antisense molecules, especially, have to hybridize with the latter regions. Static analysis using a steady-state fluorescence method clearly predicted the single-stranded regions in the folded RNA (28). However, static information is not enough when designing antisense molecules (29). If the regions are located deep in the RNA, the antisense molecule may take time to reach the region and to hybridize with it. By that time, in the competition with cellular processes such as translocation of ribosome, the antisense effect could be diminished. If the regions are located in the surface of RNA, the antisense molecules can easily hybridize with the region, and there, RNase H can promptly recognize the heteroduplex. The static analysis is quite ineffective for such evaluation, and only time-resolved luminescence anisotropy analysis using a long-lifetime luminescent probe is effective for the purpose.

In conclusion, the segmental motions of single-stranded regions of 16S rRNA were estimated by the time-resolved luminescence anisotropy analysis using a long-lifetime Ru(II) complex-labeled oligonucleotide as a probe. Results from the luminescence lifetime and luminescence quenching experiments were in good agreement with the prediction from the measurement of the segmental motions. It was predicted that the segmental motion, namely flexibility, is correlated to the depth from the surface of the 16S rRNA. Comparison between the flexibility of the single-stranded regions and the hybridization kinetics with their complementary oligonucleotides suggested a significant correlation between the flexibility and hybridization kinetics.

This research was partly supported by the Kyoto Nanotechnology Cluster of the Knowledge Cluster Initiative administrated by the Ministry of Education, Science, Sports and Culture of Japan. Support from Otsuka GEN Research Institute, administrated by Otsuka Pharmaceutical, is gratefully acknowledged.

REFERENCES

1. Ban, N., P. Nissen, J. Hansen, P. B. Moore, and T. A. Steitz. 2000. The complete atomic structure of the large ribosomal subunit at 2.4 Å resolution. *Science*. 289:905–920.
2. Clemons, W. M., Jr., J. L. May, B. T. Wimberly, J. P. McCutcheon, M. S. Capel, and V. Ramakrishnan. 1999. Structure of a bacterial 30S ribosomal subunit at 5.5 Å resolution. *Nature*. 400:833–840.
3. Carter, A. P., W. M. Clemons, D. E. Brodersen, R. J. Morgan-Warren, B. T. Wimberly, and V. Ramakrishnan. 2000. Functional insights from the structure of the 30S ribosomal subunit and its interactions with antibiotics. *Nature*. 407:340–348.
4. Augusteyn, R. C. 2004. α-crystallin: a review of its structure and function. *Clin. Exp. Optom.* 87:356–366.
5. Manley, P. W., G. Bold, J. Bruggen, G. Fendrich, P. Furet, J. Mestan, C. Schnell, B. Stolz, T. Meyer, B. Meyhack, W. Stark, A. Strauss, and J. Wood. 2004. Advances in the structural biology, design and clinical development of VEGF-R kinase inhibitors for the treatment of angiogenesis. *Biochim. Biophys. Acta*. 1697:17–27.
6. Bechinger, B., C. Aisenbrey, and P. Bertani. 2004. The alignment, structure and dynamics of membrane-associated polypeptides by solid-state NMR spectroscopy. *Biochim. Biophys. Acta*. 1666:190–204.
7. Tamm, L. K., F. Abildgaard, A. Arora, H. Blad, and J. H. Bushweller. 2003. Structure, dynamics and function of the outer membrane protein A (OmpA) and influenza hemagglutinin fusion domain in detergent micelles by solution NMR. *FEBS Lett.* 555:139–143.
8. Jao, C. C., A. Der-Sarkissian, J. Chen, and R. Langen. 2004. Structure of membrane-bound α-synuclein studied by site-directed spin labeling. *Proc. Natl. Acad. Sci. USA*. 101:8331–8336.
9. Isas, J. M., R. Langen, W. L. Hubbell, and H. T. Haigler. 2004. Structure and dynamics of a helical hairpin that mediates calcium-dependent membrane binding of annexin B12. *J. Biol. Chem.* 279: 32492–32498.
10. Tuschl, T., C. Gohlke, T. M. Jovin, E. Westhof, and F. Eckstein. 1994. A three-dimensional model for the hammerhead ribozyme based on fluorescence measurements. *Science*. 266:785–789.
11. Silverman, S. K., and T. R. Cech. 1999. RNA tertiary folding monitored by fluorescence of covalently attached pyrene. *Biochemistry*. 38: 14224–14237.

12. McCord, E. F., K. M. Morden, I. Tinoco, Jr., and S. G. Boxer. 1984. Chemically induced dynamic nuclear polarization studies of yeast tRNAPhe. *Biochemistry.* 23:1935–1939.

13. Roberts, M. F., Q. Cui, C. J. Turner, D. A. Case, and A. G. Redfield. 2004. High-resolution field-cycling NMR studies of a DNA octamer as a probe of phosphodiester dynamics and comparison with computer simulation. *Biochemistry.* 43:3637–3650.

14. Finerty, P. J., Jr., A. K. Mittermaier, R. Muhandiram, L. E. Kay, and J. D. Forman-Kay. 2005. NMR dynamics-derived insights into the binding properties of a peptide interacting with an SH2 domain. *Biochemistry.* 44:694–703.

15. Okonogi, T. M., A. W. Reese, S. C. Alley, P. B. Hopkins, and B. H. Robinson. 1999. Flexibility of duplex DNA on the submicrosecond timescale. *Biophys. J.* 77:3256–3276.

16. Simon-Lukasik, K. V., A. V. Persikov, B. Brodsky, J. A. Ramshaw, W. R. Laws, J. B. Alexander Ross, and R. D. Ludescher. 2003. Fluorescence determination of tryptophan side-chain accessibility and dynamics in triple-helical collagen-like peptides. *Biophys. J.* 84:501–508.

17. Lakowicz, J. R. 1999. Principles of Fluorescence Spectroscopy, 2nd ed. Kluwer Academic/Plenum Publishers, New York.

18. Hartshorn, R. M., and J. K. Barton. 1992. Novel dipyridophenazine complexes of Ruthenium(II): exploring luminescent reporters of DNA *J. Am. Chem. Soc.* 114:5919–5925.

19. Milton, R. C., E. Becker, S. C. Milton, J. E. Baxter, and J. F. Elsworth. 1987. Improved purities for Fmoc-amino acids from Fmoc-ONSu. *Int. J. Pept. Protein Res.* 30:431–432.

20. Meggers, E., D. Kusch, and B. Giese. 1997. An efficient synthesis of enantiomerically pure delta- and lambda-Ruthenium(II)-labeled oligonucleotides. *Helv. Chimica Acta.* 80:640–652.

21. Sullivan, B. P., D. J. Salmon, and T. J. Meyer. 1978. Mixed phosphine 2,2'-bipyridine complexes of ruthenium. *Inorg. Chem.* 17:3334–3341.

22. Terpetschnig, E., H. Szmacinski, and J. R. Lakowicz. 1995. Fluorescence polarization immunoassay of a high-molecular-weight antigen based on a long-lifetime Ru-ligand complex. *Anal. Biochem.* 227:140–147.

23. Wachter, L., J. A. Jablonski, and K. L. Ramachandran. 1986. A simple and efficient procedure for the synthesis of 5'-aminoalkyl oligodeoxynucleotides. *Nucleic Acids Res.* 14:7985–7994.

24. Gutell, R. R., N. Larsen, and C. R. Woese. 1994. Lessons from an evolving rRNA: 16S and 23S rRNA structures from a comparative perspective. *Microbiol. Rev.* 58:10–26.

25. Barton, J. K., J. M. Goldberg, C. V. Kumar, and N. J. Turro. 1986. Binding modes and base specificity of Tris(phenanthroline)ruthenium(II) enantiomers with nucleic acids: tuning the stereoselectivity. *J. Am. Chem. Soc.* 108:2081–2082.

26. Kumar, C. V., J. K. Barton, and N. J. Turro. 1985. Photophysics of Ruthenium complexes bound to double helical DNA. *J. Am. Chem. Soc.* 107:5518–5523.

27. Sakamoto, T., A. Mahara, R. Iwase, T. Yamaoka, and A. Murakami. 2005. Analytical method for estimation of kinetics of oligonucleotide/RNA hybridization using fluorescence depolarization spectroscopy. *Anal. Biochem.* 340:369–372.

28. Mahara, A., R. Iwase, T. Sakamoto, T. Yamaoka, K. Yamana, and A. Murakami. 2003. Detection of acceptor sites for antisense oligonucleotides on native folded RNA by fluorescence spectroscopy. *Bioorg. Med. Chem.* 11:2783–2790.

29. Wang, J.-Y., and K. Drlica. 2004. Computational identification of antisense oligonucleotides that rapidly hybridize to RNA. *Oligonucleotides.* 14:167–175.